Full Paper

Propellants, Explosives, Pyrotechnics

DOI: 10.1002/prep.201400239

Chromium Copper Catalysts for $LiClO_4$ Decomposition

Yanwei Zhang,[a] Ke Yan,[a] Kunzan Qiu,*[a] Jianzhong Liu,[a] Yang Wang,[b] and Junhu Zhou[a]

Abstract: Chromium copper (Cr–Cu) catalysts are well-known burning rate catalysts for solid propellants, which were used as energy source for rocket propulsion [1]. The present work reports the enhancement of lithium perchlorate ($LiClO_4$) by employing copper chromium as a catalyst. The $LiClO_4$ decomposition rate depends on the catalyst characteristics, such as chemical composition, specific surface, and crystalline structure. Scanning electron microscopy, Brunauer-Emmett-Teller, X-ray diffraction, X-ray photoelectron spectroscopy, and H_2-temperature-programmed reduction analyses were used to characterize $Cr_xCu_{(1-x)}O_{(1+0.5x)}$ catalysts. The samples are prepared using the sol-gel method with different mole ratios. Furthermore, the samples are tested to evaluate their effect on the $LiClO_4$ decomposition at various temperatures. The blank tests comparison shows that the $Cr_xCu_{(1-x)}O_{(1+0.5x)}$ catalysts strongly enhance the $LiClO_4$ decomposition. Moreover, $CuCr_2O_4$ is formed in the $Cr_xCu_{(1-x)}O_{(1+0.5x)}$ catalysts. The Cr–Cu binary composite catalysts show smaller crystallites, larger surface area, and better catalytic performance than the pure CuO samples because of the interaction of Cr and Cu ions. This study proposes a hypothetical reaction mechanism for the $LiClO_4$ catalytic decomposition of the $Cr_xCu_{(1-x)}O_{(1+0.5x)}$ catalysts.

Keywords: Copper chromite · Sol-gel · $LiClO_4$ · Catalytic decomposition

1 Introduction

Chlorates and perchlorates are usually used as oxidizing agents in pyrotechnics or propellant composites [2–4]. These oxidizers have practically and theoretically been the subject of considerable research. Lithium perchlorate ($LiClO_4$) is one of the most potential oxidizing components having the following thermal decomposition reactions:

$$\text{Main reaction}: \quad LiClO_4 \rightarrow LiCl + O_2 \tag{1}$$

$$\text{Side reaction}: \quad 4LiClO_4 \rightarrow 2Li_2O + 7O_2 + 2Cl_2 \tag{2}$$

Perchlorates are more stable than chlorates. Hence, the rapid process of reaction (1) requires a much higher temperature than chlorate requires [5]. However, this high temperature leads to the generation of trace chlorine (Cl_2), which is caused by the weak development of side reaction (2). Several catalysts are added into the composite to optimize the thermal decomposition characteristics of $LiClO_4$ and inhibit side reaction (2) [6,7]. Former researchers have reported that transition metal oxides, such as Fe_2O_3, Co_2O_3, TiO_2, MnO_2, and CuO, increase the perchlorate decomposition rate [8–13].

Although many researchers have investigated the catalytic thermal decomposition of perchlorates, the mechanisms remain inconsistent, even contradictory. Several researchers [14–16] have suggested that the only active catalysts for perchlorate decomposition are the p-type semiconductors. Other researchers (e.g. Zhang et al. [17,18]) have suggested that metal oxides containing metal cations with half-filled d orbitals probably have high activities. Zhang et al. believe that the inconsistent conclusions are probably caused by the differences in the surface areas of the additives.

Moreover, previous studies [12,18,19] have shown that both CuO and Cr_2O_3 exhibit a superior catalytic effect in perchlorate decomposition over other metal oxides. In recent years, the Cu–Cr composite oxides are commercially employed as catalysts for hydrogenation, dehydrogenation, oxidation, and alkylation [20,21]. Hence, these composite oxides have been well-known as versatile functional materials. The Cu–Cr binary catalysts have also been used as burning rate catalysts for solid propellants [22].

This study intends to investigate the catalytic effect of the $Cr_xCu_{(1-x)}O_{(1+0.5x)}$ compound catalysts on $LiClO_4$ thermal decomposition. The chromium copper catalysts in this work are synthesized using the sol-gel method with different metal ion mole ratios.

[a] *Y. Zhang, K. Yan, K. Qiu, J. Liu, J. Zhou*
State Key Laboratory of Clean Energy Utilization
Zhejiang University
Hangzhou, 310027, P. R. China
**e-mail: zhangyw@zju.edu.cn*

[b] *Y. Wang*
Institute of Advanced Technology
Zhejiang University
Hangzhou, 310027, P. R. China

2 Experimental

2.1 Catalyst Preparation

The sol-gel method was employed to synthesize the $Cr_xCu_{(1-x)}O_{(1+0.5x)}$ catalysts with $Cu(NO_3)_2 \cdot 3H_2O$, $Cr(NO_3)_3 \cdot 9H_2O$, and sucrose ($C_{12}H_{22}O_{11}$) of analytical grade. An aqueous solution was prepared by dissolving appropriate amounts of $Cu(NO_3)_2 \cdot 3H_2O$ and $Cr(NO_3)_3 \cdot 9H_2O$ in stoichiometric ratios of Cr : Cu = 1 : 0, 2 : 1, 1 : 1, 1 : 2, 0 : 1 in deionized water. Sucrose was added as a complexing agent into the prepared aqueous solution, where the mole ratio of sucrose to the total metal ions was 2 : 1. The mixed solution was then continuously stirred on a hot plate at 80 °C until it became a spongy gel. The $Cr_xCu_{(1-x)}O_{(1+0.5x)}$ gel was obtained by evaporating the remaining spongy gel moisture in an oven at 110 °C for 12 h. The dry gel was ground in an agate mortar before carbonizing at 400 °C for 3 h in a nitrogen atmosphere. The gel $Cr_xCu_{(1-x)}O_{(1+0.5x)}$ catalysts were finally obtained by calcining the carbonized gel in air at 400 °C for 4 h. The samples were cooled to room temperature in a furnace. The gel $Cr_xCu_{(1-x)}O_{(1+0.5x)}$ catalysts prepared with different mole ratios were referred to as gel Cr, gel Cr2-Cu, gel Cr-Cu, gel Cr-Cu2, and gel Cu in the remaining parts of this paper.

2.2 Catalyst Characterization

The total surface area of the $Cr_xCu_{(1-x)}O_{(1+0.5x)}$ samples was determined by performing N_2 adsorption by using an Autosorb-IQ-MP instrument (Quantachrome) based on the Brunauer-Emmett-Teller (BET) method. The samples were pretreated in a vacuum prior to the measurement at 300 °C for 2 h. The solid morphologies of the sol-gel catalysts were analyzed with a Hitachi SU-70 analytical field emission scanning electron microscope (SEM) operated at an accelerated voltage of 3.0 kV. X-ray diffraction (XRD) was performed with a D/max 2550PC with a diffracted-beam monochromator tuned to Cu-K_α radiation ($\lambda = 0.15405$ nm). The X-ray tube was operated at 40 kV and 200 mA. The scans were recorded at 0.02° intervals in the $20° \leq 2\theta \leq 80°$ range with 0.3 s count accumulation per step. The X-ray photoelectron spectra were collected with an M-Probe apparatus (Surface Science Instruments) to verify the species on the surface of the sol-gel samples. The X-ray source provided monochromatic beams by using Al-K_α radiation at 1486.6 eV and 12.5 kV. Moreover, the spectra of the Cu 2p and Cr 2p levels were recorded. All the binding energy (BE) values were calibrated using the C 1s peak at 284.8 eV. The redox cycles (i.e., TPR1/TPO/TPR2) of the various catalyst samples were performed in sequence by utilizing an automated catalyst characterization system (Micromeritics, model AutoChem. II 2920), which incorporated a thermal conductivity detector. A 2-propanol cold trap was set before the temperature-programmed reduction (TPR) process to condense the produced water vapor. A total of 40 mg of the fresh samples were pretreated at 500 °C for 1 h in a stream of argon flowing at 35 mL min^{-1}. A reducing gas of 10 % H_2 in Ar at 35 mL min^{-1} was used with a ramping temperature of 10 °C min^{-1} to 550 °C during the TPR1 sample processing. The catalysts were kept at 550 °C for 0.5 h and then further cooled to an ambient temperature. Subsequently, the samples were oxidized at 10 °C min^{-1} to 500 °C for the TPO experiment. Furthermore, the samples were maintained at 500 °C for 2 h with a 2 % O_2 in N_2 mixed gas. The TPR measurements were carried out again after cooling the samples to ambient temperature in an argon flow.

2.3 Activity Measurement

The $LiClO_4$ catalytic decomposition was performed in a fixed-bed continuous flow stainless reactor (30 mm diameter) at atmospheric pressure. One gram of the catalyst was used after being homogeneously mixed with an appropriate volume of coarse quartz particles (i.e., 40–80 mesh). The schematic diagram of the experimental equipment for $LiClO_4$ catalytic decomposition is displayed in Figure 1. The reactor was purged with nitrogen to remove all the oxygen prior to the experiments. The catalyst was heated to 360 °C to 420 °C, thereafter. The starting material (i.e., $LiClO_4$ powder) was introduced into the reactor with a screw feeder at a fixed mass flow. The $LiClO_4$ powder was carried by nitrogen with a flow rate of 100 mL min^{-1}, melted, and dropped on the catalyst layer. The decomposition reaction of the fused $LiClO_4$ was carried out on the surface of the sol-gel catalysts. Furthermore, the solid product (i.e., co-melting LiCl-$LiClO_4$ [23]) was condensed in the condenser, which was cooled by circulating water. The trace Cl_2 in the gas phase generated by side reaction (2) was trapped in the NaOH scrubber. Afterwards, the wet gas out of the NaOH scrubber was dried in the silica gel scrubber and the O_2 gas was analyzed using an oxygen analyzer. The $LiClO_4$

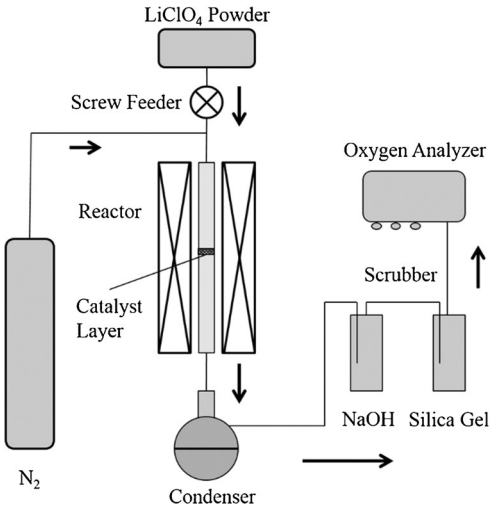

Figure 1. Schematic diagram of the experimental catalyst activity test system.

conversion was calculated by the quantity of O_2 measured with respect to the theoretical yield of oxygen.

3 Results and Discussion

3.1 BET Measurement

The specific surface areas, average pore diameters, and pore volumes of the sol-gel catalysts measured by N_2 adsorption by the BET method are shown in Table 1.

The gel Cu catalyst showed the smallest BET surface area (0.5 $m^2 g^{-1}$) and pore volume (4.44×10^{-3} $mL g^{-1}$) (Table 1), whereas the gel Cr sample exhibited the largest surface area (56.9 $m^2 g^{-1}$) and pore volume (3.82×10^{-1} $mL g^{-1}$). The two monometal oxide catalysts showed similar parameters for the average pore diameter.

A comparison with the gel Cu and the binary compound metal oxide catalysts illustrated that the introduction of chromic oxide considerably optimized the structural catalytic properties. The pore volume rapidly increased from 7.29×10^{-2} $mL g^{-1}$ to 2.93×10^{-1} $mL g^{-1}$ when the mole ratio of chrome was increased. The binary catalysts also exhibited a much larger BET surface area than the gel Cu sample, whereas the gel Cr-Cu catalyst had a smaller surface area than the gel Cr-Cu2. The gel Cr2-Cu had the largest BET surface and pore volume of the compound catalysts.

3.2 XRD Analysis

The catalytic crystalline structures were investigated by XRD measurements. The XRD patterns of the $Cr_xCu_{(1-x)}O_{(1+0.5x)}$ catalysts are presented in Figure 2. Accordingly, the XRD profiles changed with various mole ratios. The gel Cu catalyst showed a single CuO phase [24]. The characteristic peaks corresponding to the CuO phase decreased when the chromium ratio increased. Moreover, the new characteristic peaks of the $CuCr_2O_4$ spinel and Cr_2O_3 phases increased [22]. Only the Cr_2O_3 phase was detected for the catalytic profile of the gel Cr. The XRD peaks of the gel Cu sample were very sharp, which indicated the presence of large crystallites. The other catalysts were rather broad, which implied the existence of small crystallites. The poor microscopic structure of the gel Cu restricted its catalytic performance. The crystallite size reduction of the binary catalysts was probably caused by the interaction of Cr and Cu ions or the $CuCr_2O_4$ phase formation.

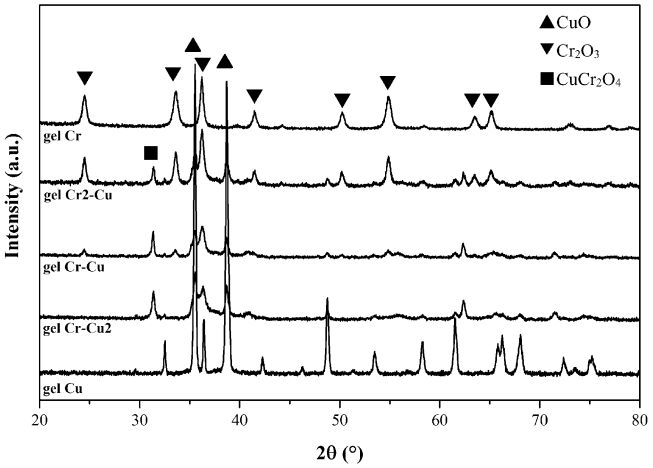

Figure 2. XRD patterns of the catalysts prepared via the sol-gel method.

Table 1. Structural properties of the sol-gel catalysts determined by N_2 adsorption-desorption.

Samples	BET surface area S_{BET} [$m^2 g^{-1}$]	Pore volume V_p [a)] [$mL g^{-1}$]	Average pore diameter [b)] [nm]
Gel Cu	0.5	4.44×10^{-3}	39.03
Gel Cr-Cu2	18.8	7.29×10^{-2}	15.48
Gel Cr-Cu	15.3	2.40×10^{-1}	62.80
Gel Cr2-Cu	31.2	2.93×10^{-1}	37.62
Gel Cr	56.9	3.82×10^{-1}	28.88

a) Barret-Joyner-Halenda cumulative desorption pore volume. b) Mean pore diameter $= 4\ V_p/S_{BET}$.

3.3 Scanning Electron Microscopy (SEM) Studies

SEM was employed to investigate the catalytic morphology. The typical SEM images of the gel Cu, gel Cr-Cu2, gel Cr-Cu, gel Cr2-Cu, and gel Cr are displayed in Figure 3a–e. The gel Cu catalyst (Figure 3a) exhibited a morphology characterized by large agglomerates, whereas the gel Cr sample (Figure 3e) showed a stack of an irregular rod-like structure. The different morphologies of the gel Cu and gel Cr were coincidental with the XRD profiles in Figure 2. A comparison of the three binary catalysts (Figure 3b–d) showed various pore structures and sample morphologies with different chromium and copper mole ratios. The gel Cr-Cu2 (Figure 3b) showed a smooth surface with the smallest pore diameter. The gel Cr-Cu had a rough surface with many

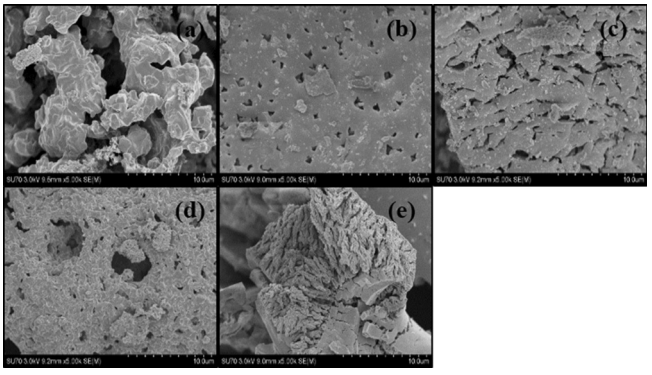

Figure 3. SEM micrographs of (a) gel Cu, (b) gel Cr-Cu2, (c) gel Cr-Cu, (d) gel Cr2-Cu, and (e) gel Cr.

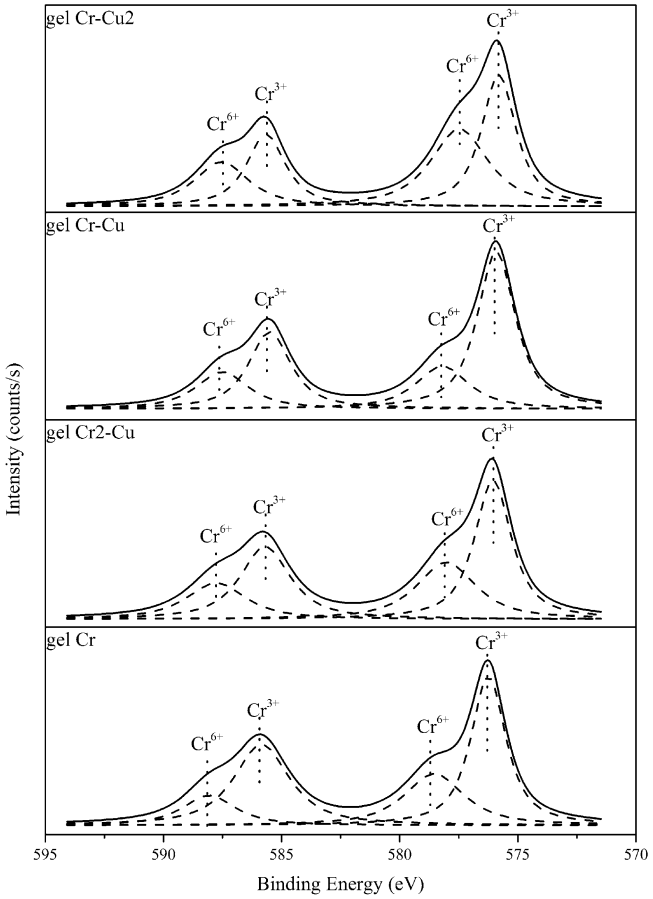

Figure 4. XPS Cr 2p spectra of the gel Cr-Cu2, gel Cr-Cu, gel Cr2-Cu, and gel Cr samples.

cracks (Figure 3c) and an irregular structure with many tiny holes is exhibited in gel Cr2-Cu (Figure 3d).

3.4 X-ray Photoelectron Spectroscopy (XPS) Analysis

The chemical nature of the active species present on the surface was important for the establishment of the catalytic properties. Accordingly, an XPS analyses were performed to obtain information on the surface composition and the chemical state of the $Cr_xCu_{(1-x)}O_{(1+0.5x)}$ catalysts prepared via the sol-gel method.

The XPS patterns of the gel Cr-Cu2, gel Cr-Cu, gel Cr2-Cu, and gel Cr samples for the core level Cr 2p spectra are shown in Figure 4. Both Cr^{6+} and Cr^{3+} were clearly visible in the sol–gel catalyst spectra, which presented four peak assignments (Figure 4). The Cr $2p_{3/2}$ signal corresponding to the catalysts was decomposed into two contributions at around 576.4 and 579.0 eV, which were characteristic of Cr^{3+} and Cr^{6+}, respectively [25]. Meanwhile, the two peaks near 585.9 and 588.2 eV in the Cr $2p_{1/2}$ spectra were associated with Cr^{3+} and Cr^{6+}, respectively. The fitted peak areas in the XPS spectra (Figure 4) were used to estimate the quantity of Cr^{6+} in Cr^{3+} in these catalysts. The calculated

Table 2. Chemical state analysis of the catalysts prepared via the sol-gel method. The data were determined from the XPS spectra.

Samples	Cu 2p I_a/I_{pp} [%]	Cr 2p Cr^{6+}/Cr^{3+} [%]
Gel Cr	–	47.23
Gel Cr2-Cu	69.56	61.61
Gel Cr-Cu	40.51	44.87
Gel Cr-Cu2	38.08	90.61
Gel Cu	0	–

Cr^{6+}/Cr^{3+} ratios for the catalysts are shown in Table 2. The Cr^{6+}/Cr^{3+} ratios greatly changed with different Cr contents, which were probably affected by $CuCr_2O_4$ formation. The gel Cr-Cu2 and gel Cr2-Cu samples exhibited much larger Cr^{6+}/Cr^{3+} ratios than that of the gel Cr catalyst. The gel Cr-Cu sample showed a slightly smaller Cr^{6+}/Cr^{3+} ratio than the gel Cr sample. This comparison implied that the proper addition of copper oxide into chromic oxide suppressed Cr^{6+} ion formation.

The Cu 2p XPS spectra of the gel Cr2-Cu, gel Cr-Cu, gel Cr-Cu2, and gel Cu samples are illustrated in Figure 5. The comparison of the Cu 2p XPS profiles of the binary catalysts

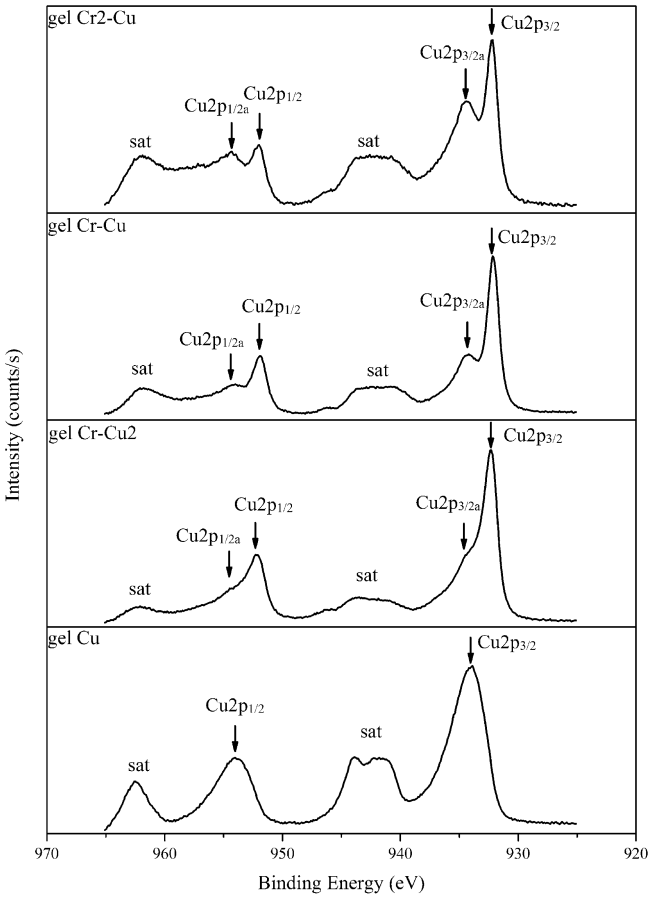

Figure 5. XPS Cu 2p spectra of the gel Cr2-Cu, gel Cr-Cu, gel Cr-Cu2, and gel Cu samples.

Table 3. TPR results for the catalysts prepared via the sol-gel method.

Sample	Peak temperature [°C]				Hydrogen consumption [mol g^{-1}]			
	TPR1		TPR2		TPR1		TPR2	
	$T_{p,L}$	$T_{p,H}$	$T_{p,L}$	$T_{p,H}$	M_L	M_H	M_L	M_H
Gel Cr	165.8	502.3	172.9	364.7	3.49×10^{-3}	3.21×10^{-3}	8.17×10^{-3}	1.44×10^{-3}
Gel Cr2-Cu	208.5	210.1	383.6	370.1	5.75×10^{-4}	6.81×10^{-4}	4.36×10^{-4}	1.47×10^{-3}
Gel Cr-Cu	176.5	474.4	187.2	365.6	4.04×10^{-3}	3.35×10^{-3}	9.67×10^{-3}	1.51×10^{-3}
Gel Cr-Cu2	163.6	498.0	174.0	366.7	3.06×10^{-3}	2.08×10^{-3}	5.75×10^{-3}	1.62×10^{-3}
Gel Cu	264.8	393.7	229.9	370.2	1.56×10^{-2}	5.79×10^{-4}	1.55×10^{-2}	1.52×10^{-3}

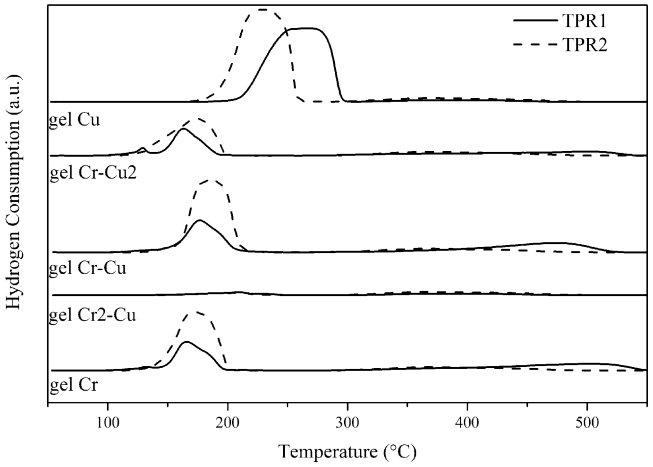

Figure 6. TPR1 and TPR2 profiles of the catalysts prepared via the sol-gel method.

and that of the gel Cu sample showed that the principal Cu $2p_{1/2}$ and Cu $2p_{3/2}$ peaks shifted toward a lower binding energy. The corresponding shoulder peaks (i.e., Cu $2p_{1/2a}$ and Cu $2p_{3/2a}$, respectively) simultaneously appeared thereafter. Based on the standard BE, the strong Cu $2p_{1/2}$ and Cu $2p_{3/2}$ peaks of the composite catalysts were characteristic of the Cu^{2+} ions. In addition, the shoulder peaks Cu $2p_{1/2a}$ and Cu $2p_{3/2a}$ corresponded to the existence of the Cu^0 species [26]. Separating the characteristic peaks was difficult because of the existing shake-up satellites (i.e., sat peaks). The Cu^0/Cu^{2+} ratio was investigated by determining the ratio of the intensities of the shoulder peaks to those of the principal peaks (i.e., I_a/I_{pp}). Furthermore, estimating the accurate Cu^0/Cu^{2+} ratio was hard because of the photoreduction in the spectrometer [27]. The I_a/I_{pp} ratios, however, provided valuable information for the comparison between catalysts. The I_a/I_{pp} ratios are shown in Table 2, where the intensity ratios (i.e., I_a/I_{pp}) increased from 38.08 % to 69.56 % when the Cr/Cu catalytic mole ratios increased from 1 : 2 to 2 : 1. The addition of chromium oxide in the catalysts increased the Cu^0/Cu^{2+} mole ratio. Moreover, the Cu^0 species content in the samples was consistent with the catalytic activity.

The catalytic activity of the samples increased with I_a/I_{pp} ratios, whereas the Cr^{6+}/Cr^{3+} ratios showed an irregular trend (Table 2).

3.5 H_2-TPR Cycle Studies

TPR1/TPO/TPR2 cycle studies were performed to investigate the reversibility of the sol-gel catalysts in a redox cycle. The TPR1 and TPR2 profiles of these samples are shown as solid and dash lines, respectively, in Figure 6. All the TPR assays proved that two reduction bands exist between room temperature and 550 °C. The bumpy low-temperature reduction peaks in the TPR profiles corresponded to the reduction of copper and chrome. By contrast, the flat high-temperature reduction peaks were characteristic of the reduction of bulk metal oxides or copper chromate species [26, 28]. The most significant results in terms of peak temperatures and hydrogen consumptions of the reduction peaks are summarized in Table 3. The comparison of the monometal oxide catalysts showed that the sample gel Cu exhibited a much higher low-peak temperature $T_{p,L}$ than the gel Cr. $T_{p,l}$ of the binary catalysts were between that of the gel Cu and the gel Cr. However, $T_{p,L}$ increased from 163.6 °C in gel Cr-Cu2 to 208.5 °C in gel Cr2-Cu as the chrome content increased, thereby exhibiting a reverse $T_{p,H}$ trend. This phenomenon implied that a small amount of chrome decreased $T_{p,L}$. The contrary effect appeared as the chrome content increased. $T_{p,L}$ shifted to a higher temperature after a TPR/TPO cycle, whereas $T_{p,H}$ moved toward a lower temperature. The shift was probably caused by the further interaction of copper and chrome during the redox process.

According to M_L in Table 3, introducing chrome decreased the hydrogen reduction consumption, which was mostly due to $CuCr_2O_4$ formation (Figure 2) [29]. The gel Cr2-Cu composition was optimal for $CuCr_2O_4$ synthesis. In addition, the low-temperature hydrogen consumption was significantly less than the others. In contrast with TPR1, the gel Cu sample presented a passivation in M_L of TPR2. Moreover, the gel Cr catalyst exhibited growth in M_L. All the binary samples except gel Cr2-Cu also expanded in the low-temperature hydrogen consumption during TPR2.

According to the preceding TPR analyses, the gel Cr2-Cu sample showed an unsatisfying performance in terms of the redox properties. However, the sample exhibited the best catalytic activity in $LiClO_4$ conversion, which proved that the $LiClO_4$ decomposition over $Cr_xCu_{(1-x)}O_{(1+0.5x)}$ did not depend on the catalytic redox properties.

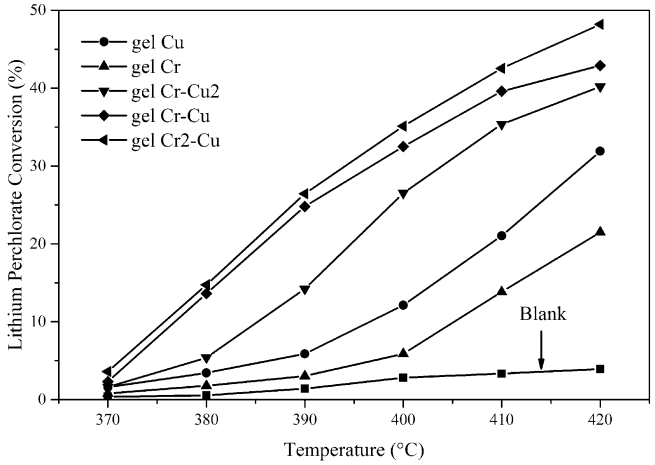

Figure 7. $LiClO_4$ conversion for the $Cr_xCu_{(1-x)}O_{(1+0.5x)}$ catalysts prepared via the sol-gel method.

3.6 Catalytic Performances for $LiClO_4$ Decomposition

The catalytic activities of the samples with different Cr and Cu mole ratios were assessed in the $LiClO_4$ decomposition between 370 °C and 420 °C. The $LiClO_4$ conversions with various temperatures for the sol-gel $Cr_xCu_{(1-x)}O_{(1+0.5x)}$ catalysts are shown in Figure 7. The uncatalyzed (blank) conditions are also provided for comparison (Figure 7).

The $LiClO_4$ conversions in all the experiments increased with the reaction temperature, which indicated that the temperature strongly affected the reaction rate. The highest conversion for the blank tests was far below 5%, which implied that $LiClO_4$ was very stable at the experimental temperature range. All the catalysts significantly improved the $LiClO_4$ conversion compared with the blank yield. The comparison of the monometal oxide catalysts showed that the gel Cu sample showed a better catalytic activity than the gel Cr catalyst even with much less specific surface areas. The binary metal oxide catalysts exhibited a much better catalytic activity than the single-component catalyst (Figure 7). Furthermore, the gel Cr2–Cu experiments showed the optimal catalytic properties among all the catalysts. The sample obtained a conversion of 48.2% at 420 °C. The gel Cr-Cu sample exhibited a similar $LiClO_4$ conversion with the gel Cr2-Cu catalyst, but a gap grew with the temperature increased. The gel Cr-Cu2 sample provided a poorer result, particularly for temperatures below 400 °C.

3.7 Hypothetic Mechanism Analysis of $LiClO_4$ Decomposition

The key factor for the stable oxy-anions of chlorine (i.e., ClO_4^-, ClO_3^-, ClO_2^-, and ClO^-) was the π-bonding extension in these compounds. The oxyanion stability increased with the oxidation state of chlorine when the symmetry decreased the anion instability as follows [5]:

$$ClO_4^- > ClO_3^- > ClO_2^- > ClO^- \quad (3)$$

Reaction (1) proceeded in two steps. First, ClO_4^- decomposed into ClO_3^- and O_2 (reactions (4) and (5)) [30]. Second, ClO_3^- decomposed following the mechanism proposed by Rudloff and Freeman [31] (reactions (6) and (7)). The reactions are as follows:

$$ClO_4^- \rightarrow ClO_3^- + O \quad (4)$$

$$2O \rightarrow O_2 \quad (5)$$

$$2ClO_3^- \rightarrow ClO_4^- + ClO_2^- \quad (6)$$

$$ClO_2^- \rightarrow Cl^- + O_2 \quad (7)$$

As shown in formula (3), ClO_4^- was more stable than ClO_3^-. The first step in reaction (4) was considered as the rate-determining step. Hence, this work focused on the mechanism of step one. Based on the results of a previous study [32] and the present work, we suggest that the Cu^0 species should be the active sites. The Cu^0 species easily lost and gained electrons, which indicated that it can easily accept and get rid of oxygen atoms. Furthermore, a hypothetical mechanism was accordingly proposed (Figure 8).

The molten ClO_4^- was absorbed on Cu^0 and one oxygen atom of the perchlorate was attracted to the active sites before the reaction. The Cl–O bond linked to the trapped oxygen atom slowly weakened and was then cleaved (reaction (4)). ClO_3^- from the former process detached from the catalyst surface and then decomposed (reactions (6) and (7)). The isolate active atoms promptly combined into O_2 (reaction (5)).

In summary, the key process of the decomposition reaction should be the first Cl–O bond breakage in ClO_4^-. The catalysts offered the active site, Cu^0, to promote this mechanism.

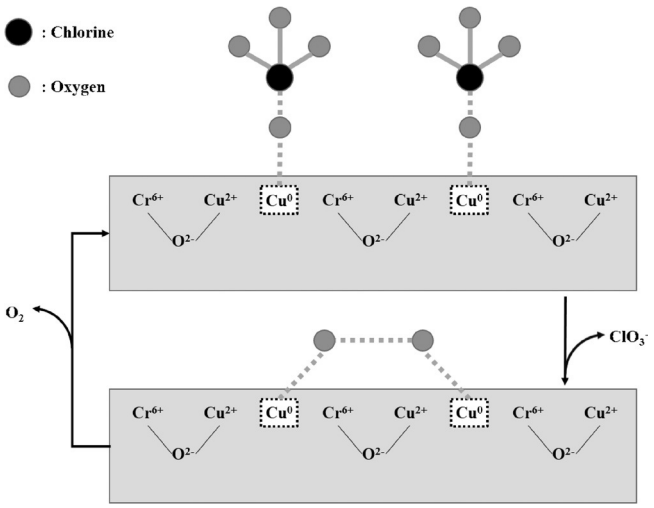

Figure 8. Proposed mechanism of the $LiClO_4$ catalytic decomposition of $Cr_xCu_{(1-x)}O_{(1+0.5x)}$.

4 Conclusions

This study aimed to discover the enhanced catalytic effect of the Cr-Cu composite catalyst on the $LiClO_4$ decomposition. The $Cr_xCu_{(1-x)}O_{(1+0.5x)}$ catalysts prepared via the sol-gel method exhibited excellent catalytic effects in the $LiClO_4$ decomposition. The catalysts were characterized via BET, XRD, SEM, XPS, and H_2-TPR cycle analyses.

The BET characterizations proved that the introduction of chrome expanded the specific surface areas and pore volume. The XRD profiles confirmed that the existence of chrome restrained crystal growth. The BET features coincided with the microstructure of the catalysts investigated via SEM. The XPS analysis of the Cu 2p spectra confirmed that the Cu^0 species content in the catalysts was associated with the catalytic activity. However, the hydrogen consumption from the H_2-TPR cycle analysis in Table 3 was not in agreement with the catalytic activity on the $LiClO_4$ decomposition. Therefore, the active sites of the catalyst should be related to the Cu^0 species. Finally, a hypothetical mechanism of the $LiClO_4$ catalytic decomposition over $Cr_xCu_{(1-x)}O_{(1+0.5x)}$ was proposed.

References

[1] E. Campos, R. Dutra, L. Rezende, M. Faria Diniz, W. Massae Dio Nawa, K. Iha, Performance Evaluation of Commercial Copper Chromites as Burning Rate Catalyst for Solid Propellants, *J. Aerospace Technol. Management* **2010**, *2*, 323 – 330.

[2] D. Ouyang, G. Pan, H. Guan, C. Zhu, X. Chen, Effect of Different Additives on the Thermal Properties and Combustion Characteristics of Pyrotechnic Mixtures Containing the $KClO_4$/Mg–Al Alloy, *Thermochim. Acta* **2011**, *513*, 119–123.

[3] C.-G. Zhu, H.-Z. Wang, L. Min, Ignition Temperature of Magnesium Powder and Pyrotechnic Composition, *J. Energ. Mater.* **2013**, *31*, 219 – 226.

[4] E.-C. Koch, Special Materials in Pyrotechnics: III. Application of Lithium and Its Compounds in Energetic Systems, *Propellants Explos. Pyrotech.* **2004**, *29*, 67–80.

[5] S. G. Hosseini, S. M. Pourmortazavi, S. S. Hajimirsadeghi, Thermal Decomposition of Pyrotechnic Mixtures Containing Sucrose with Either Potassium Chlorate or Potassium Perchlorate, *Combust. Flame* **2005**, *141*, 322 – 326.

[6] S. H. Ba, Z. X. Sun, Z. Zhang, C. H. Zhang, Studied Catalysis of CuO Nanocrystal on $KClO_4$ Decomposition, *Adv. Mater. Res.* **2011**, *335–336*, 128–131.

[7] Y. L. Zhu, H. Huang, H. Ren, Q. J. Jiao, Effects of Aluminum Nanoparticles on Thermal Decomposition of Ammonium Perchlorate, *J. Korean Chem. Soc.* **2013**, *57*, 109–114.

[8] J.-S. Lee, C.-K. Hsu, The DSC Studies on the Phase Transition, Decomposition and Melting of Potassium Perchlorate with Additives, *Thermochim. Acta* **2001**, *367–368*, 367 – 370.

[9] V. Patel, Sonoemulsion Synthesis of Long CuO Nanorods with Enhanced Catalytic Thermal Decomposition of Potassium Perchlorate, *J. Cluster Sci.* **2013**, *24*, 821 – 828.

[10] M. A. Stephens, E. L. Petersen, D. L. Reid, R. Carro, S. Seal, Nano Additives and Plateau Burning Rates of Ammonium-Perchlorate-Based Composite Solid Propellants, *J. Propul. Power* **2009**, *25*, 1068 – 1078.

[11] L.-l. Liu, G.-q. He, Y.-h. Wang, Effect of Oxidizer on the Combustion Performance of Boron-Based Fuel-Rich Propellant, *J. Propul. Power* **2014**, *30*, 285–289.

[12] H. Qin, M. Zha, Z. Ma, F. Zhao, S. Xu, H. Xu, Controllable Fabrication of CuO/Ammonium Perchlorate (AP) Nanocomposites through Ceramic Membrane Anti-Solvent Recrystallization, *Propellants Explos. Pyrotech.* **2014**, *39*, 694 – 700.

[13] Z. Ma, F. Li, H. Bai, Effect of Fe_2O_3 in Fe_2O_3/AP Composite Particles on Thermal Decomposition of AP and on Burning Rate of the Composite Propellant, *Propellants Explos. Pyrotech.* **2006**, *31*, 447–451.

[14] T. Wydeven, Catalytic Fecomposition of Dodium Chlorate, *J. Catal.* **1970**, *19*, 162 – 171.

[15] W. K. Rudloff, E. S. Freeman, The Catalytic Effect of Metal Oxides on Thermal Decomposition Reactions. II. The Catalytic Effect of Metal Oxides on the Thermal Decomposition of Potassium Chlorate and Potassium Perchlorate as Detected by Thermal Analysis Methods, *J. Phys. Chem.* **1970**, *74*, 3317 – 3324.

[16] E. S. Freeman, D. A. Anderson, Effects of Radiation and Doping on the Catalytic Activity of Magnesium Oxide on the Thermal Decomposition of Potassium Perchlorate, *Nature* **1965**, *205–208*, 378–379.

[17] J. C. Cannon, Y. C. Zhang, Catalytic Fecomposition of Potassium Chlorate, *J. Therm. Anal.* **1994**, *41*, 981 – 993.

[18] Y. Zhang, G. Kshirsagar, J. E. Ellison, J. C. Cannon, Catalytic Effects of Metal Oxides on the Decomposition of Potassium Perchlorate, *Thermochim. Acta* **1996**, *278*, 119 – 127.

[19] L. Chen, L. Li, G. Li, Synthesis of CuO Nanorods and Their Catalytic Activity in the Thermal Decomposition of Ammonium Perchlorate, *J. Alloys Compd.* **2008**, *464*, 532–536.

[20] P. S. Sathiskumar, C. R. Thomas, G. Madras, Solution Combustion Synthesis of Nanosized Copper Chromite and Its Use as a Burn Rate Modifier in Solid Propellants, *Ind. Eng. Chem. Res.* **2012**, *51*, 10108 – 10116.

[21] Q. Geng, X. Zhao, X. Gao, S. Yang, G. Liu, Low-Temperature Combustion Synthesis of $CuCr_2O_4$ Spinel Powder for Spectrally Selective Paints, *J. Sol-Gel Sci. Technol.* **2012**, *61*, 281–288.

[22] A. M. Kawamoto, L. C. Pardini, L. C. Rezende, Synthesis of Copper Chromite Catalyst, *Aerospace Sci. Technol.* **2004**, *8*, 591–598.

[23] M. M. Markowitz, D. A. Boryta, The Decomposition Kinetics of Lithium Perchlorate, *J. Phys. Chem.* **1961**, *65*, 1419 – 1424.

[24] M. A. Stephens, E. L. Petersen, R. Carro, D. L. Reid, S. Seal, Multi-Parameter Study of Nanoscale TiO_2 and CeO_2 Additives in Composite AP/HTPB Solid Propellants, *Propellants Explos. Pyrotech.* **2010**, *35*, 143–152.

[25] M. Crivello, C. Pérez, J. Fernández, G. Eimer, E. Herrero, S. Casuscelli, E. Rodríguez-Castellón, Synthesis and Characterization of Cr/Cu/Mg Mixed Oxides obtained from Hydrotalcite-Type Compounds and their Application in the Dehydrogenation of Isoamylic Alcohol, *Appl. Catal. A* **2007**, *317*, 11–19.

[26] Z. Wang, J. Xi, W. Wang, G. Lu, Selective Production of Hydrogen by Partial Oxidation of Methanol over Cu/Cr Catalysts, *J. Mol. Catal. A* **2003**, *191*, 123 – 134.

[27] P.-O. Larsson, A. Andersson, L. R. Wallenberg, B. Svensson, Combustion of CO and Toluene; Characterisation of Copper Oxide Supported on Titania and Activity Comparisons with Supported Cobalt, Iron, and Manganese Oxide, *J. Catal.* **1996**, *163*, 279 – 293.

[28] S. K. Das, P. Mohanty, S. Majhi, K. K. Pant, CO-Hydrogenation over Silica-Supported Iron-Based Catalysts: Influence of Potassium Loading, *Appl. Energy* **2013**, *111*, 267–276.

[29] B. M. Nagaraja, A. H. Padmasri, P. Seetharamulu, K. Hari Prasad Reddy, B. David Raju, K. S. Rama Rao, A Highly Active Cu-MgO-Cr_2O_3 Catalyst for Simultaneous Synthesis of Furfuryl Alcohol and Cyclohexanone by a Novel Coupling Route – Combination of Furfural Hydrogenation and Cyclohexanol Dehydrogenation, *J. Mol. Catal. A* **2007**, *278*, 29–37.

[30] J. L. de la Fuente, Mesoporous Copper Oxide as a New Combustion Catalyst for Composite Propellants, *J. Propul. Power* **2013**, *29*, 293 – 298.

[31] W. K. Rudloff, E. S. Freeman, The Catalytic Efect of Metal Oxides on Thermal-Decomposition Reactions. I. The Mechanism of the Molten-Phase Thermal Decomposition of Potassium Chlorate in Mixtures with Potassium Chloride and Potassium Perchlorate, *J. Phys. Chem.* **1969**, *73*, 1209 – 1215.

[32] M. Zhang, G. Li, H. Jiang, J. Zhang, Investigation on Process Mechanism on Cu–Cr Catalysts for Ethanol Dehydrogenation to Ethyl Acetate, *Catal. Lett.* **2011**, *141*, 1104 – 1110.

Received: October 7, 2014
Published online: December 9, 2014

